PHILOSOPHICAL TRANSACTIONS OF THE ROYAL SOCIETY B BIOLOGICAL SCIENCES

Why the chameleon has spiral–shaped muscle fibres in its tongue

Johan L. Van Leeuwen

Phil. Trans. R. Soc. Lond. B 1997 **352**, 573-589
doi: 10.1098/rstb.1997.0039

Why the chameleon has spiral-shaped muscle fibres in its tongue

JOHAN L. VAN LEEUWEN

Department of Physiology, Leiden University, Wassenaarseweg 62, PO Box 9604, NL-2300 RC Leiden, The Netherlands (j.l.van_leeuwen@physiology.medfac.leidenuniv.nl)
Institute for Sport Science, LSB Biomechanics, Friedrich Schiller University, Seidelstraße 20, D-07749 Jena, Germany

CONTENTS

SUMMARY

The intralingual accelerator muscle is the primary actuator for the remarkable ballistic tongue projection of the chameleon. At rest, this muscle envelopes the elongated entoglossal process, a cylindrically shaped bone with a tapering distal end. During tongue projection, the accelerator muscle elongates and slides forward along the entoglossal process until the entire muscle extends beyond the distal end of the process. The accelerator muscle fibres are arranged in transverse planes (small deviations are possible), and form (hitherto unexplained) spiral-shaped arcs from the peripheral to the internal boundary.

To initiate tongue projection, the muscle fibres probably generate a high intramuscular pressure. The resulting negative pressure gradient (from base to tip) causes the muscle to elongate and to accelerate forward. Effective forward sliding is made possible by a lubricant and a relatively low normal stress exerted on the proximal cylindrical part of the entoglossal process. A relatively high normal stress is, however, probably required for an effective acceleration of muscle tissue over the tapered end of the process. For optimal performance, the fast extension movement should occur without significant (energy absorbing) torsional motion of the tongue. In addition, the tongue extension movement is aided by a close packing of the muscles fibres (required for a high power density) and a uniform strain and work output in every cross-section of the muscle.

A quantitative model of the accelerator muscle was developed that predicts internal muscle fibre arrangements based on the functional requirements above and the physical principle of mechanical stability. The curved shapes and orientations of the muscle fibres typically found in the accelerator muscle were accurately predicted by the model. Furthermore, the model predicts that the reduction of the entoglossal radius towards the tip (and thus the internal radius of the muscle) tends to increase the normal stress on the entoglossal bone.

1. INTRODUCTION

Chameleonid lizards capture prey by a rapid projection of the tongue out of the mouth over the remarkable distance of more than one body length. Tongue projection occurs in 30–50 ms, depending on body size and prey distance (Bell 1990). The morphology of the feeding apparatus (e.g. Houston 1828; Brücke 1852; Gnanamuthu 1930; Bell 1989), the electrical activity of the muscles involved (Wainwright & Bennett 1992*a*), and the mechanism of tongue projection (e.g. Duvernoy 1836; Brücke 1852; Zoond 1933; Altevogt & Altevogt 1954; Gans 1967; Bell 1989, 1990; Wainwright *et al.* 1991), recently reviewed and extended by Wainwright & Bennett (1992*a*, *b*), have received considerable attention. Quantitative models of the architectural characteristics of the system and the dynamics of the tongue projection process are, however, lacking. Recent progress with related problems of skeletal muscle design (Van Leeuwen & Spoor 1992, 1993) and tentacle extension in squid (Van Leeuwen & Kier 1997) have opened new perspectives

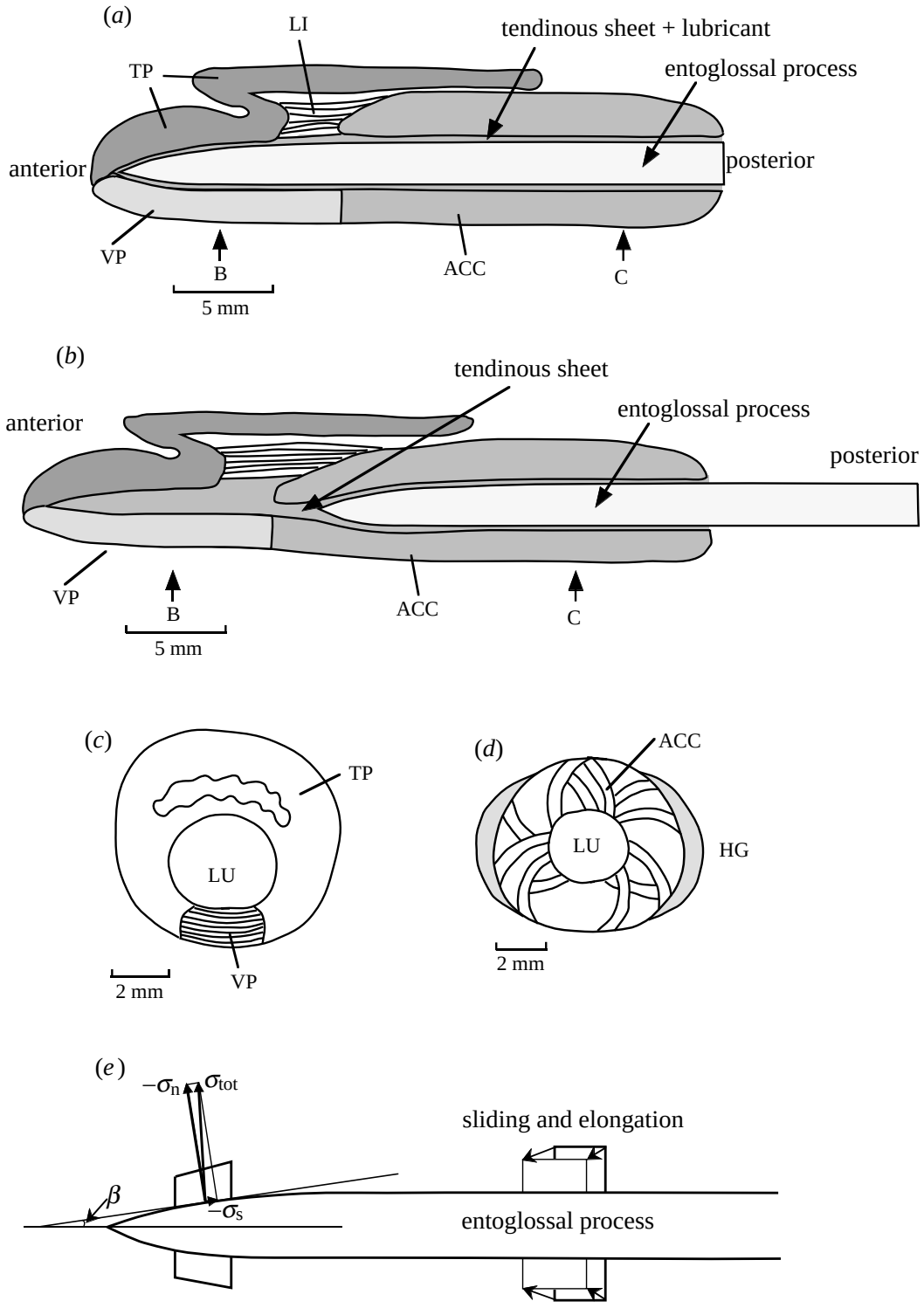

Figure 1. Illustration of the tongue pad and accelerator muscle of the chameleon tongue. (*a*) Diagram of a para-sagittal section through the tongue of a chameleon (*Chameleo jacksonii*). (*b*) Similar to (*a*), but now the accelerator muscle is elongated, and it extends partly beyond the tip of the entoglossal process. (*c*) Diagram of a cross-section at arrow B in diagram (*a*). (*d*) Diagram of a cross-section at arrow C in diagram (*a*). Note the curved paths of the muscle fibres. (*e*) Diagram of entoglossal process with two parts of accelerator muscle. At the right-hand side, a muscle block is shown in original position (normal line thickness) and after muscle elongation and sliding (thin lines). At the left-hand side, force components are depicted from tapering part of entoglossal process on muscle segment. The total force of the bone on the muscle part is positive (directed distally) if $\sigma_n \sin\beta - \sigma_s \cos\beta > 0$, where β is the angle of taper and assuming a uniform stress distribution. Diagrams (*a*), (*c*) and (*d*) are loosely based on a figure from Wainwright & Bennett (1992*a*) and histological sections of Bell (1989). Abbreviations: ACC, accelerator muscle; HG, hyoglossal muscle; LI, longitudinal adductor muscle; TP, membrana glandulosa of tongue pad; VP, ventral projection of accelerator muscle; σ_s, frictional stress, directed parallel to surface of entoglossal process; σ_n, normal stress, directed at right angles to surface of entoglossal process; σ_{tot}, local stress component from entoglossal process on muscle.

for quantitative predictions for the chameleon tongue apparatus.

To aid in understanding the model developed in this paper, I shall first summarize the morphology and previously proposed propulsion mechanisms of the chameleon tongue (figure 1). More detailed discussions can be found, for example, in Brücke (1852), Gnanamuthu (1930, 1937), Bell (1989) and Wainwright & Bennett (1992*a*, *b*). Structures that connect to the tongue will not be discussed. The accelerator muscle of the tongue is mounted on the elongate and cylindrically shaped cartilaginous entoglossal process (also denoted as entoglossal bone (figure 1*a*)). The diameter of the entoglossal process is remarkably constant over much of its length (Wainwright & Bennett 1992*b*), except for the distal part, the pars entoglossa, which is tapered. The pars entoglossa is flexible and terminates in a collagenous sheet. This sheet is continuous with a fairly thick bilayered collagenous sheet which envelops the entoglossal process. Between the sheet and the entoglossal process, a viscous fluid is present which is thought to serve as a lubricant (Gans 1967; Bell 1989).

Anteriorly, the tongue consists mainly of the tongue pad (figure 1*a*). Ventrally, the tongue pad is connected to the most anterior part (approximately 35% of the muscle length) of the accelerator muscle. This muscle part is *not* active immediately before and during the forward acceleration phase of the tongue (Wainwright & Bennett 1992*a*). The muscle fibres in the anterior accelerator muscle run as short arcs in transverse planes (figure 1*c*). The fibres make an angle of about 90° with the radial direction.

More posteriorly, the accelerator muscle is cylindrical in shape with a central lumen that accommodates the bilayered collageneous sheet and the entoglossal process. This portion was identified by Brücke (1852) to be the main actuator for tongue extension, and was indeed found to be electrically active just before and during the main acceleration phase of the tongue (Wainwright & Bennett 1992*a*). Wainwright & Bennett (1992*a*) argued that the muscle may become electrically silent even before the onset of projection. For practical purposes, the onset of tongue projection was, however, identified as the first video field in which the tongue had travelled more than 5 mm. With 200 fields s^{-1}, this corresponds to a velocity greater or equal to 1 m s^{-1}. It is clear that, in this definition, projection onset was immediately *after* the main acceleration phase of the tongue when the highest muscle forces would be expected. Therefore, I prefer to choose an earlier instant for the projection onset (estimated value depends on event, range approximately 30–70 ms). If one also considers the electromechanical delay in relaxation, it is clear that the muscle is highly mechanically active while in contact with the entoglossal process.

Interestingly, the muscle fibres in the main portion of the accelerator muscle run also in transverse planes, but here they follow curved paths between the outer and the inner surface, either clockwise or anticlockwise (Gnanamuthu 1930; Gans 1967; Bell 1989; figure 1*d*). The angle that the muscle fibres make with the radial direction and their curvature vary along their length. The accelerator muscle has often been viewed as a sphincter muscle (e.g. Zoond 1933). This functional property will be re-examined in the present paper. At the peripheral boundary, the muscle fibres attach to a thin tendinous sheet (figure 5*h*).

During tongue projection, the main part of the accelerator muscle contracts radially, elongates and slides forward along the entoglossal process (figure 1*e*). Radial contraction of the muscle must be accompanied by elongation because muscle tissue is almost incompressible (Abbott & Baskin 1962). An especially strong forward acceleration is achieved when the muscle slides over the tapering end of the entoglossal process (Wainwright & Bennett 1992*b*). The reaction force from the tapering entoglossal process on the muscle is presumably directed in a forward direction, thanks to the low friction force caused by the lubricant. A piece of muscle tissue is accelerated forward by the reaction force from the entoglossal process if $\sigma_n \sin\beta > \sigma_s \cos\beta$, where σ_n is the normal stress from the muscle on the process (inward direction defined positive), σ_s the shearing stress from the muscle on the process produced by friction (distal direction defined positive) and β is the angle of the surface of the process with the longitudinal direction (cf. figure 1*e*).

The final tongue shortening is considerably slower than the tongue projection and occurs presumably partly by elastic counter forces and partly by active muscle forces in the hyoglossal muscle (figure 1*d*, Wainwright & Bennett 1992*b*), which has longitudinally arranged muscle fibres. Tongue retraction will not be further discussed in this paper.

To analyse the architecture of the accelerator muscle in relation to the extension process, I wish to formulate the following functional and architectural requirements for rapid tongue extension.

(1) Muscle elongation is facilitated by a strongly negative pressure gradient along the accelerator muscle from base to tip, analogous to the situation in the muscular stalks of the tentacles of squid (Van Leeuwen & Kier 1997). Thus, the accelerator muscle should be able to produce considerable internal muscle pressures. The highest pressure should be produced at the base of the muscle.

(2) The portions of the accelerator muscle that slide over the cylindrical part of the entoglossal process should exert a relatively low normal (i.e. at right angles to the surface and directed inwards) stress on the entoglossal process. Too high a normal stress may increase friction with the entoglossal process and retard sliding, especially somewhat later in projection as higher speeds are attained. This last requirement may set a limit to the sphincter function of the muscle. A typical sphincter with concentric layers of muscle fibres cannot uncouple the normal stress and the intramuscular pressure and would therefore be disadvantageous. The allowed normal stress through time will depend on the properties of the lubricant (which are still unknown).

PHILOSOPHICAL TRANSACTIONS OF THE ROYAL SOCIETY B BIOLOGICAL SCIENCES

(3) Muscle parts that slide over the tapering portion of the entoglossal process should exert a high enough normal stress on the process so as to obtain a substantial forward reactive force from the process, thereby helping to accelerate the tongue forward. Thus, it may be advantageous if the normal stress on the entoglossal process increases from the cylindrical to the tapering part of the entoglossal process.

(4) The muscle fibres in the accelerator muscle should operate with fairly constant strains over their length. Additionally, the fibre strain should be fairly constant throughout the muscle tissue since the muscle fibres are presumably all of one very fast type. Thus, work output per unit volume should be fairly constant throughout the muscle tissue. This principle was outlined by Van Leeuwen & Spoor (1992, 1993).

(5) The muscle fibres in the accelerator muscle should be closely packed so as to obtain a high power density for the available tissue mass. This principle was also outlined by Van Leeuwen & Spoor (1992, 1993).

(6) An extremely fast extension movement should be possible without significant (energy absorbing) torsional motion of the accelerator muscle.

Using these six requirements, I attempt for the first time to predict quantitatively the shape of the muscle fibre trajectories in the accelerator muscle. I also discuss whether the accelerator muscle could rapidly increase the normal stress on the entoglossal process while sliding from the cylindrical to the conical part.

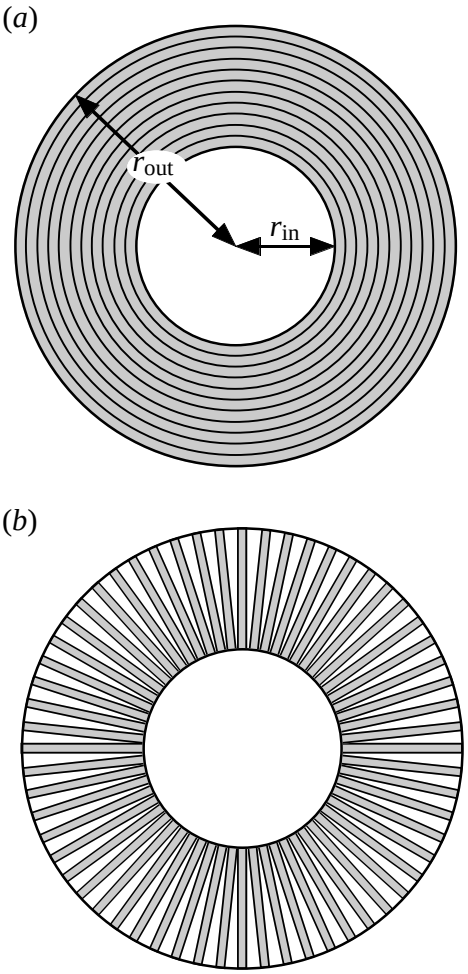

Figure 2. Illustration of two theoretical designs that are *not* present in the chameleon tongue. (*a*) Design as a typical sphincter muscle with concentric muscle fibre layers around the entoglossal process. An excellent packing of the muscle fibres is realized, but the innermost layers cannot do much work along the cylindrical part of the entoglossal process. The normal stress on the entoglossal bone is very high and may even be limiting for the sliding function. (*b*) Second theoretical design with radially directed muscle fibres. The requirement for a good packing of the muscle fibres is violated and the normal stress on the entoglossal process would be negative. This last property prohibits a good acceleration over the tapering end of the entoglossal process. The spaces between the radial fibres could in principle be filled with tapering muscle fibres.

2. MODEL ANALYSIS AND RESULTS

The symbols used in this section are summarized in Appendix 1. For development of a high intramuscular pressure and rapid tongue projection, it is optimal if the muscle fibres in the accelerator muscle are arranged in transverse planes. This is similar to the fibre arrangement of the extensor muscles of squid tentacles (Van Leeuwen & Kier 1997), which also can generate a purely longitudinal extension. A transverse orientation ensures that the longitudinal component of the principal muscle fibre tensile stress is initially zero. During tongue extension, the muscle fibres may deviate slightly from the ideal transverse orientation due to forward velocity differences between the inner and outer boundary. The muscle fibres generate a longitudinal intramuscular pressure gradient, which causes the accelerator muscle to lengthen.

In the following model, a transverse configuration of the muscle fibres will be assumed. I will also assume that the entoglossal process and the accelerator muscle are axisymmetric with respect to the central longitudinal axis. Thus, both elements have cross-sectional areas with circular outer shapes. The inner radius of the accelerator muscle r_{in} is assumed to be equal to the outer radius of the collagenous sheet that envelopes the entoglossal process (figures 2*a*, 3*a*). In the model, I will consider the inner tendinous sheet to be part of the entoglossal process, unless otherwise stated. Let r_{out} be the outer radius of the accelerator muscle, and $\alpha_f = \alpha_f(r)$ the angle of a muscle fibre with the radial direction at radius r. The radius is measured with respect to the common central axis of the entoglossal process and the accelerator muscle. The muscle tissue is assumed to be incompressible.

The muscle fibre stress σ_f is defined as the tensile stress that would be generated in the longitudinal direction of a muscle fibre without a local fluid pressure p. The relation between longitudinal muscle fibre stress σ_l, σ_f, and p is as follows:

$$\sigma_l = \sigma_f - p. \quad (1)$$

In the discussion that follows, I will calculate pres-

sure distributions in transverse planes under the assumption that inertial components (mass accelerations) can be neglected. In general, this assumption is not allowed when dealing with predictions of motion in the chameleon tongue. In Appendix 2, it is shown that, in the pressure gradient formula (30), the acceleration term is much smaller than the tensile muscle fibre stress term. The acceleration term can therefore be neglected in the pressure calculations. However, the tensile muscle fibre stress σ_f depends (nonlinearly) on the strain and strain rate. Therefore, I will only consider pressure distributions normalized with respect to σ_f. These normalized values were judged sufficient for the present purpose of predicting muscle fibre trajectories.

It is instructive to discuss first two possible muscle fibre arrangements which have distinct disadvantages. The first option is to arrange the fibres in circular paths around the entoglossal process (figure 2*a*). Thus, $\alpha_f = 90°$ at every point in the muscle. This is the design of a typical sphincter muscle. Although this design provides a very good packing of the muscle fibres (requirement 5), it has also two major disadvantages. First, the muscle fibre layers adjacent to the entoglossal process cannot shorten very much along the cylindrical part of the process. Therefore, initially they cannot do much work and do not contribute substantially to the forward acceleration of the tongue. Second, the normal stress exerted on the cylindrical part of the entoglossal process would be very high and equal to the intramuscular pressure at the inner boundary. This could be a hindrance for the longitudinal sliding movement of the tongue due to frictional forces. I cannot yet evaluate quantitatively the importance of this factor because no data are available on the friction between muscle and entoglossal process as a function of normal stress and sliding velocity. The normal stress on the process can be calculated if it is assumed that a muscle fibre of thickness $\mathrm{d}r$ and local curvature $c_f = 1/R_f$ (R_f = local fibre radius of curvature) generates a pressure difference (Van Leeuwen & Spoor 1992)

$$\mathrm{d}p = -\sigma_f c_f \,\mathrm{d}r \tag{2}$$

over its cross-section in the direction opposite to the curvature vector. The intramuscular pressure at radius r can now be approximated by

$$p_1 = -\int_{r_{out}}^{r} \sigma_f c_f \,\mathrm{d}r, \tag{3}$$

neglecting inertial components and assuming an ambient pressure of zero. So, the pressure at the outer muscle boundary is zero. If σ_f is uniform throughout the muscle tissue, then (3) reduces to $\sigma_f \ln(r_{out}/r)$, yielding a normal stress $\sigma_{n,1}$ on the entoglossal process of $p_{1,r_{in}} = \sigma_f \ln(r_{out}/r_{in})$. In this design, the innermost muscle layers can be squeezed inwards by the outer layers. This must lead to a strain increase in the longitudinal tongue direction since local muscle volume is almost constant. The normal stress on the entoglossal process is positive (directed inwards), and equal to the muscle pressure at the inner boundary:

$$\sigma_{n,1} = p_{1,r_{in}}. \tag{4}$$

The second extreme design option is a radial arrangement of straight muscle fibres (figure 2*b*). Thus, $\alpha_f = 0°$ at every point in the muscle. In such an arrangement, considerable interfibre spaces occur, especially at the periphery of the muscle. Thus, the close packing requirement is violated. An advantage of this arrangement is the much more homogeneous pressure distribution in a transverse section. If inertial effects and ambient pressure components are ignored once again, and assuming a constant muscle fibre stress, it can be shown that the pressure gradient in the radial direction is zero if the influence of the radial acceleration is neglected (figure 3*a*, *b* and Appendix 2). From a force balance requirement at the outer boundary, the intramuscular pressure can now be calculated from

$$p_2 = \frac{r_{in}\sigma_f}{r_{out}}, \tag{5}$$

where it is assumed that the muscle fibre stress is uniform, and where an average stress is assumed in the radial direction. The average radial tensile stress is assumed to vary in proportion to $1/r$. Now, a pressure differential is present across the outer muscle boundary. The normal stress on the entoglossal process is negative (directed outwards), and is equal to

$$\sigma_{n,2} = p_2 - \sigma_f. \tag{6}$$

A negative normal stress is disadvantageous because it prohibits the generation of a forwardly directed reaction force from the tapering end of the entoglossal process to the tongue. Because of the negative normal stress, the accelerator muscle would tend to dilate. This would, however, probably be prevented by a counteracting negative pressure in the lubricant and inner tendinous sheet.

The disadvantage of the first design of the limited shortening for the innermost layers has now vanished; sarcomeres close to the entoglossal process can shorten because the local longitudinal strain (i.e. in the longitudinal direction of the tongue) in the muscle tissue can increase. A close packing could be realized if the fibres would taper towards the inner boundary. Apart from force transmission problems, this would still lead to inappropriate normal stress on the entoglossal process.

In conclusion, the two extreme designs do not fulfil all functional requirements of the tongue projection mechanism. The design that (closely) fulfils all functional demands is likely to be an intermediate between these two extremes. I shall now try to predict this optimal design. The requirement of close packing of the muscle fibres will be considered first. It will be assumed that each muscle fibre (or muscle fibre bundle) runs uninterrupted from the inner boundary to the outer boundary of the accelerator muscle.

Consider now a muscle fibre with angle $\alpha_{f,r_{in}}$ at the inner boundary (figure 4). The muscle fibre is assumed to have a constant cross-sectional area over its

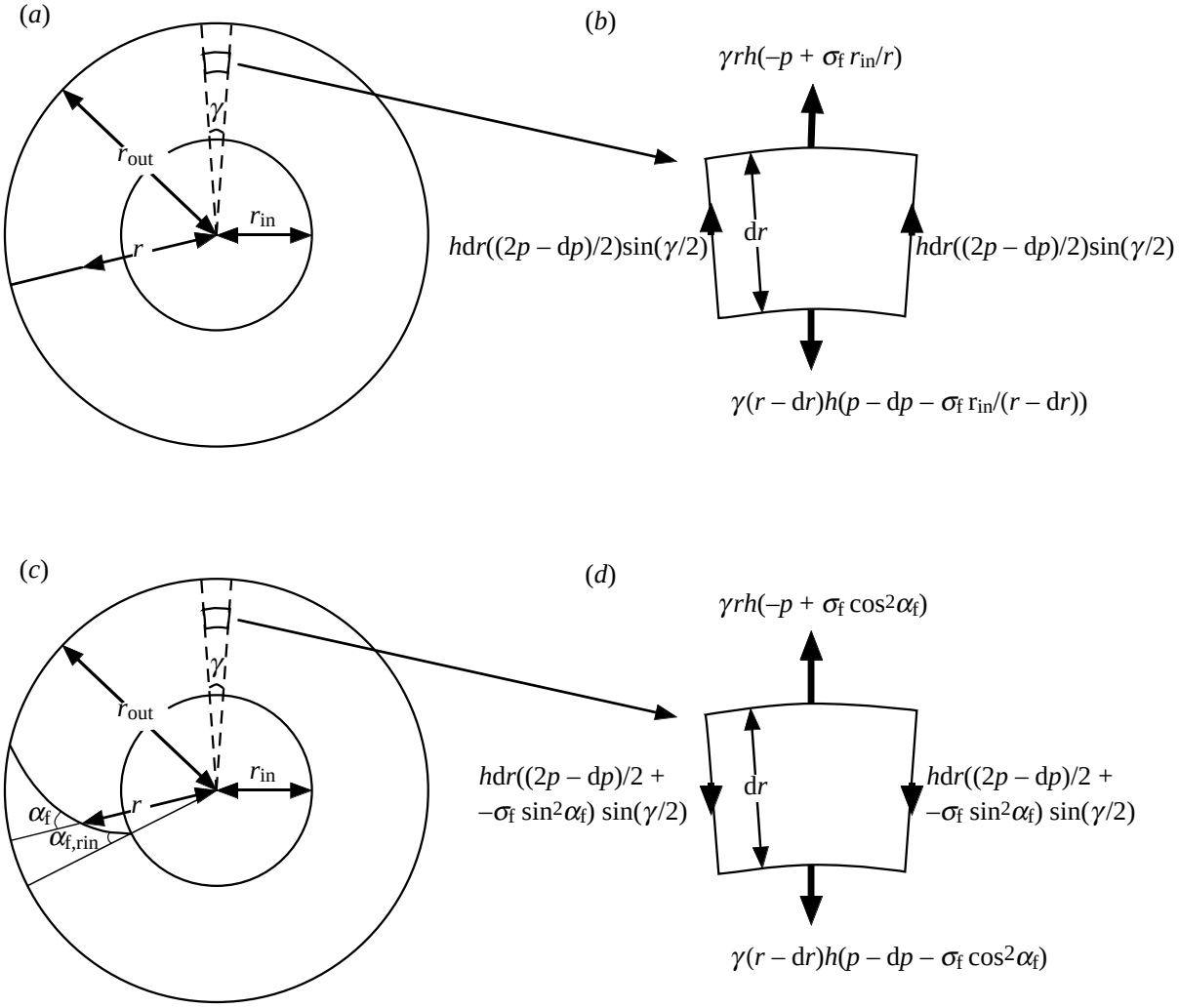

Figure 3. (*a*) Design 2 with radially oriented muscle fibres. (*b*) Force components in the outward direction on an infinitesimally small tissue block with thickness dr in radial direction and h in longitudinal direction of tongue. Ignoring inertial components, the sum of the force components should be zero. After some algebra it follows that d$p = 0$ (Appendix 2). (*c*) Design 3 with variable orientation of muscle fibres according to optimal packing criterion. (*d*) Free-body diagram for the calculation of the pressure jump dp over an infinitesimally thin curved sheet with thickness dr. After some algebra and ignoring inertial components, equation (17) is obtained (Appendix 2).

length. This agrees with an effective force transmission. The width h_f (in the longitudinal direction of the tongue) of the muscle fibre is also assumed to be constant over the length because all muscle fibres run in transverse planes. The same holds for the width d_f in the transverse plane. In the transverse plane, the muscle fibre is attached over the following distance to the inner boundary:

$$g_{f,r_{in}} = \frac{d_f}{\cos\alpha_{f,r_{in}}}, \tag{7}$$

where it is assumed that $g_{f,r_{in}} \ll 2\pi r_{in}$. Similarly, let the length $g_f = g_f(r)$ by which each imaginary circle (with radius r, $r_{in} \leq r \leq r_{out}$) traverses the muscle fibre be equal to

$$g_f = \frac{d_f}{\cos\alpha_f}. \tag{8}$$

A complete filling of the muscle with muscle fibres requires now that

$$g_f = g_{f,r_{in}} \frac{r}{r_{in}}. \tag{9}$$

From these last three formulae it can be derived that

$$\alpha_f = \arccos\left(\frac{r_{in}}{r}\cos\alpha_{f,r_{in}}\right). \tag{10}$$

Thus, α_f is completely determined by r_{in} and $\alpha_{f,r_{in}}$, and the whole fibre trajectory can be easily computed from the conditions at the inner boundary. Figure 5 shows seven examples of muscle fibre trajectories that fulfil the close packing demand (requirement 5). The value of $\alpha_{f,r_{in}}$ varies in the range 0–88°. Of course, the $\alpha_{f,r_{in}} = 88°$ solution is very similar to the typical sphincter muscle ($\alpha_{f,r_{in}} = 90°$, cf. figure 2*a*). The observed muscle fibre trajectories in the chameleon (figure 5*h*), as deduced from histological sections made by Gans (1967) and Bell (1989), are remarkably close to figures 5*c*, *d*, and in general

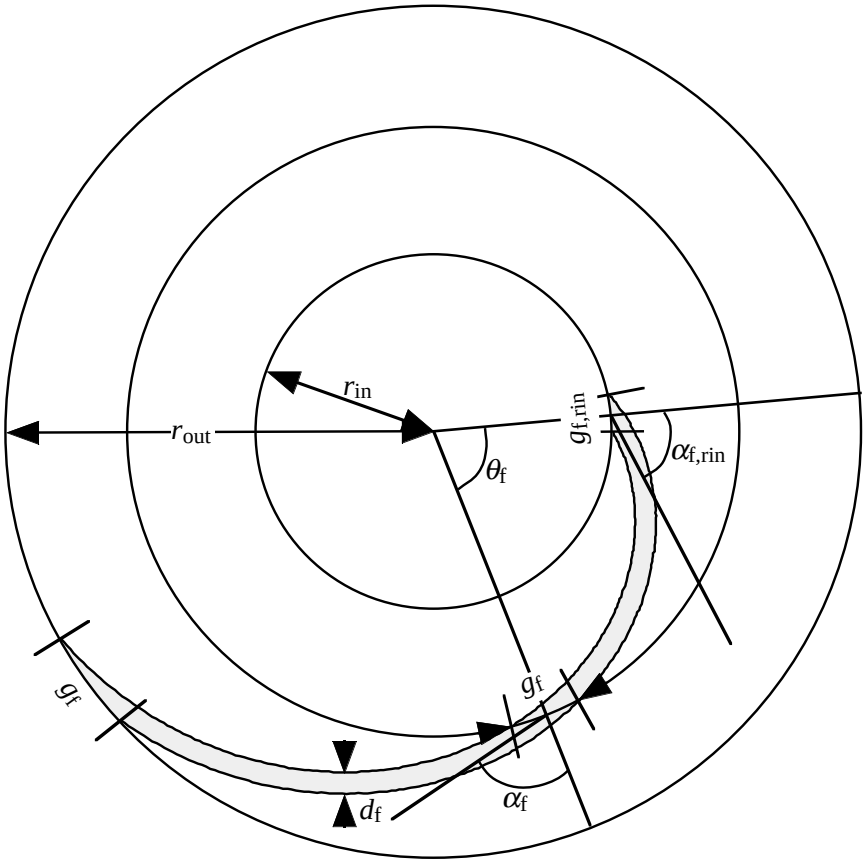

Figure 4. Diagram for calculation of fibre trajectory for close packing designs according to equation (10). The value of $\alpha_{f,r_{in}}$ is 60°. Further explanations in the text.

histological sections show fibre arrangements in the range of figure 5*b–d*. At present, a detailed quantitative comparison between predicted and observed muscle fibre trajectories is not yet useful due to the significant distortions in the histological sections.

If all muscle fibres are arranged either clockwise or anticlockwise, the accelerator muscle would always make a rotational movement along its longitudinal axis. The requirement of a limited torsional motion (6) can be easily fulfilled if equal numbers of muscle fibres run clockwise and anticlockwise. Such an arrangement is observed in drawings and photographs from histological sections found in Gnanamuthu (1930, 1937) and Bell (1989). I measured the surface ratio of all clockwise and all anticlockwise oriented muscle fibres in four complete histological cross-sections (table 1). The values found were all close to the expected value of one. Future work is planned to carry out a more rigorous test.

With α_f, the curvature of the muscle fibres is also determined. Let s_f be a curvilinear distance coordinate along the muscle fibre. Then, it holds that

$$c_f = \frac{1}{R_f} = \frac{d\theta_f + \alpha_f)}{ds_f} = \frac{d\theta_f}{ds_f} + \frac{d\alpha_f}{dr} \Big/ \frac{ds_f}{dr}, \qquad (11)$$

where, for a particular muscle fibre, θ_f is the angle between the radial direction at r and the radial direction at r_{in} ($\theta_f \geq 0$). Using (10), it can be derived

Table 1. *Measured ratios of clockwise and anticlockwise muscle fibres*

source	ratio
1	1.141
2	1.050
3	0.993
4	1.016

Sources: 1, Gnanamuthu (1930), text figure 11; 2, Gnanamuthu (1930), text figure 15; 3, Gnanamuthu (1937), text figure 38; 4, Bell (1989), figure 7B.

that

$$\frac{d\alpha_f}{dr} = \frac{d \arccos((r_{in}/r)\cos\alpha_{f,r_{in}})}{dr} = \frac{r_{in}\cos\alpha_{f,r_{in}}}{r^2\sqrt{1-(\cos\alpha_{f,r_{in}} r_{in}/r)^2}}, \qquad (12)$$

and

$$\frac{ds_f}{dr} = \frac{1}{\cos\alpha_f} = \frac{r}{r_{in}\cos\alpha_{f,r_{in}}}. \qquad (13)$$

Furthermore,

$$\frac{d\theta_f}{ds} = \frac{\sin\alpha_f}{r} = \frac{\sin\arccos((r_{in}/r)\cos\alpha_{f,r_{in}})}{r}. \qquad (14)$$

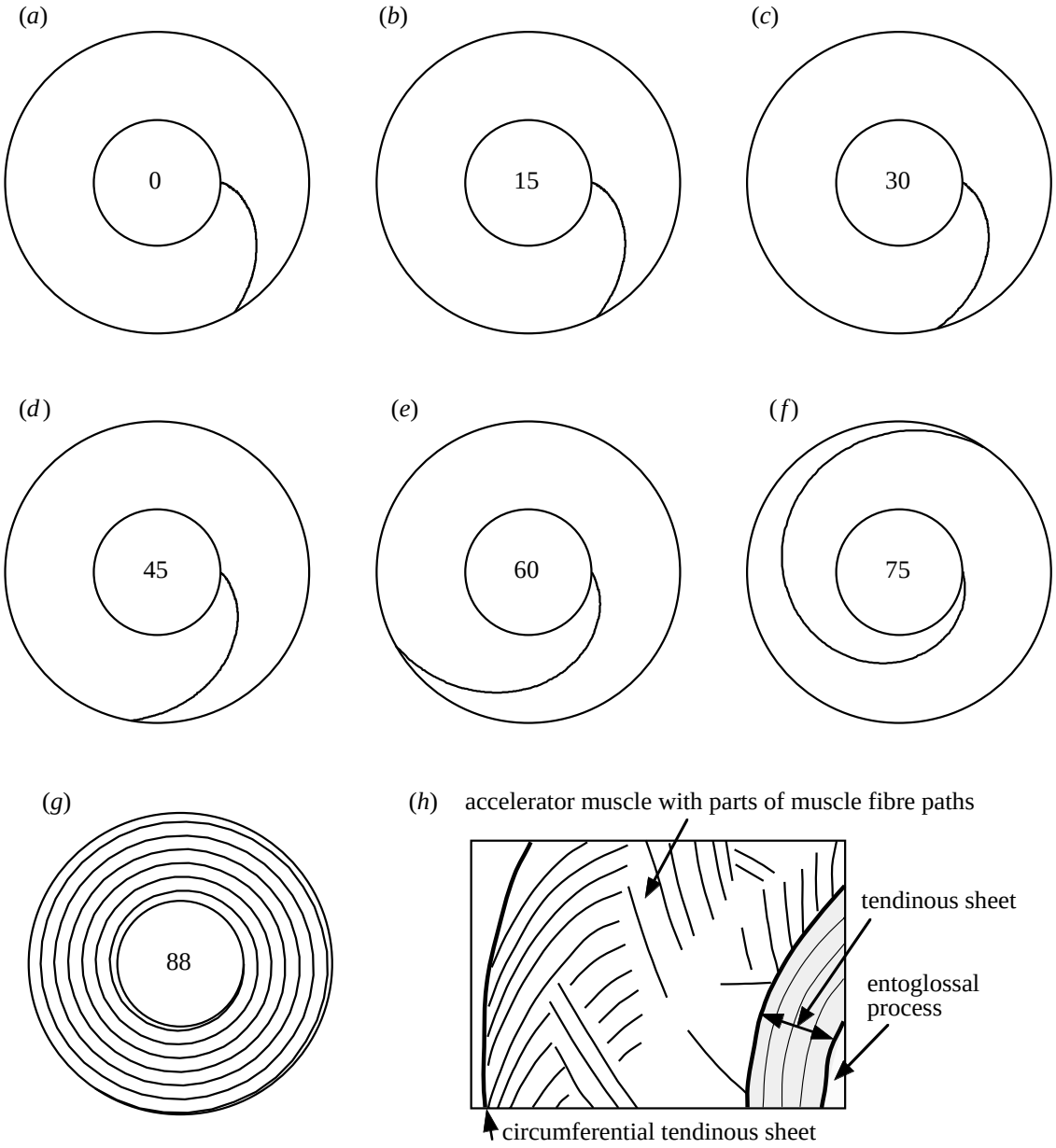

Figure 5. (*a*)–(*g*) Family of architectural designs according to equation (10) with an excellent packing of the muscle fibres. The value of $\alpha_{\mathrm{f},r_{\mathrm{in}}}$ is respectively 0, 15, 30, 45, 60, 75, and 88° for panels (*a*)–(*g*). (*h*) Drawing based on an approximately transverse histological section through the base of the tongue by Gans (1967). Directions of muscle fibres parts are indicated by pieces of arcs in clockwise and anti-clockwise directions. Fibres paths could not be followed over their complete length. It is found that in several cases $\alpha_{\mathrm{f},r_{\mathrm{in}}} \approx 45°$. In a few cases, a somewhat smaller angle is present. Note the thick tendinous sheet that envelops the entoglossal process.

By substituting (12), (13), and (14) into (11), it follows that

$$c_{\mathrm{f}} = \frac{\sin \arccos((r_{\mathrm{in}}/r)\cos\alpha_{\mathrm{f},r_{\mathrm{in}}})}{r} + \frac{r_{\mathrm{in}}^2 \cos^2\alpha_{\mathrm{f},r_{\mathrm{in}}}}{r^3\sqrt{1-(\cos\alpha_{\mathrm{f},r_{\mathrm{in}}} r_{\mathrm{in}}/r)^2}}. \qquad (15)$$

Thus, muscle fibre curvature is largest at the inner boundary and smallest at the outer boundary. The calculated muscle fibre trajectories are therefore spiral shaped. This corresponds to the fibre paths in histological sections (e.g. Gans 1967, Bell 1989). Furthermore, c_{f} increases with a decrease in $\alpha_{\mathrm{f},r_{\mathrm{in}}}$. The curvature predictions are illustrated in figure 6*a*, where, for a number of values of $\alpha_{\mathrm{f},r_{\mathrm{in}}}$, non-dimensional fibre curvature ($c_{\mathrm{f}}^* = c_{\mathrm{f}} r_{\mathrm{in}}$) is plotted against non-dimensional radius (r/r_{in}).

I shall consider to what extent the pressure and force requirements 1–3 can be met with a close packing design with limited torsion. Therefore, the pressure distribution inside the muscle has to be calculated. The intramuscular pressure at the outer boundary should balance the radial tensile stress of the muscle fibres and can therefore be calculated as

$$p_{r_{\mathrm{out}}} = \sigma_{\mathrm{f}} \cos^2 \alpha_{\mathrm{f},r_{\mathrm{out}}}, \qquad (16)$$

where it is assumed that the surface tension is zero. The squared cosine is needed because (i) the muscle

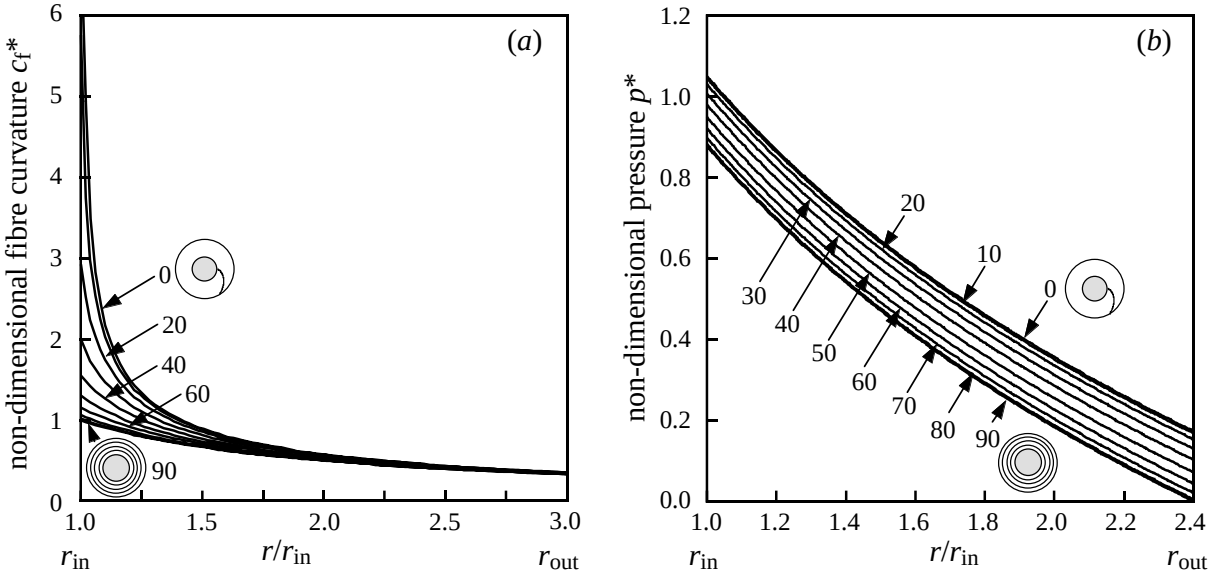

Figure 6. (*a*) Non-dimensional muscle fibre curvature ($c_f^* = c_f r_{in}$) against r_{out}/r_{in}. A family of curves is shown with the angle $\alpha_{f,r_{in}}$ as parameter (values given in degrees). For $\alpha_{f,r_{in}} = 0$ and $r \to r_{in}$, $c_f^* \to \infty$ (see equation (15)). Pictograms for $\alpha_{f,r_{in}} = 0$ and 90° depict cross-sections of entoglossal process (grey) and muscle (white), with muscle fibre path(s). (*b*) Similar family of curves as shown in panel (*a*), but now for non-dimensional pressure ($p^* = p/\sigma_f$) against r_{out}/r_{in}.

fibre inward force is proportional to the fibre thickness d_f, which equals the peripheral attachment distance times $\cos\alpha_{f,r_{out}}$, and (ii) the force component perpendicular to the circumference must be considered, and equals muscle fibre force times $\cos\alpha_{f,r_{out}}$. Muscle fibres are very thin tubes with in principle a free fluid connection over their length. Most fluid is, however, bound to proteins. Therefore, it can safely be assumed that during the very short force development process, pressure equalization along the muscle fibre is insignificant and therefore can be neglected. Hence, pressure contours can make an angle with the muscle fibre direction. With the assumption of a uniform muscle fibre stress over the muscle volume, the pressure contours are a family of concentric circles in the transverse plane. The pressure differential dp in the (*outward*) radial direction over an infinitesimally thin curved sheet of thickness dr (centred around the origin) is calculated as (figure 3*c*, *d* and Appendix 2)

$$\mathrm{d}p = -\frac{\sigma_f}{r}\,\mathrm{d}r. \tag{17}$$

Quite interestingly, this equation leads, with the same uniform muscle fibre stress, to the same pressure gradient as in the typical sphincter muscle (compare with equation (2)). Thus, the pressure gradient is invariant with a change in $\alpha_{f,r_{in}}$ (with σ_f held constant). Now, $p = p(r)$ can be calculated as

$$p = p_{r_{out}} - \int_{r_{out}}^{r} \frac{\sigma_f}{r}\,\mathrm{d}r. \tag{18}$$

Formula (18) reduces to (3) if $\alpha_{f,r_{in}} = 90°$. Thus, the highest intramuscular pressure is generated with the lowest $\alpha_{f,r_{in}}$ (and identical muscle fibre stresses), because this provides the greatest pressure differential ($p_{r_{out}}$) at the outer boundary. The pressure distribution (made non-dimensional through division by σ_f) in a muscle with $r_{out} = 2.4r_{in}$, which is a typical dimension, is shown for different $\alpha_{f,r_{in}}$ in figure 6*b*. As expected from equation (18), the pressure gradient decreases with an increasing r.

The normal stress σ_n on the entoglossal process is calculated as

$$\sigma_n = p_{r_{out}} - \int_{r_{out}}^{r_{in}} \frac{\sigma_f}{r}\,\mathrm{d}r - \sigma_f \cos^2\alpha_{f,r_{in}}, \tag{19}$$

where a squared cosine is again needed for the reasons explained previously. The third term represents the reducing effect of the inner muscle fibre stress (which causes an outward pull). Figure 7 shows contours of the normal stress (made again non-dimensional by division by σ_f) on the entoglossal bone. The vertical axis shows the inner fibre angle $\alpha_{f,r_{in}}$, and the horizontal axis shows the ratio of outer and inner radius. Each point in the contour plot represents one particular muscle design. In the positive normal stress range, the normal stress increases with an increase in $\alpha_{f,r_{in}}$, and also with an increase of r_{out}/r_{in} (and thus muscle thickness). At the extreme left side, no muscle is present and the normal stress is therefore zero. Quite interestingly, in the lower left corner an area of negative normal stress is present. This design range represents fairly thin muscles with $\alpha_{f,r_{in}} < 45°$. The area is widest at the bottom since here the outward pull of the muscle fibres is greatest. The contour of zero normal stress has a bifurcation point for $\alpha_{f,r_{in}} = 45°$ and $r_{out}/r_{in} = 1$.

With a fairly small (0–40°) inner fibre angle $\alpha_{f,r_{in}}$, a relatively high intramuscular pressure can be generated in combination with a fairly moderate normal

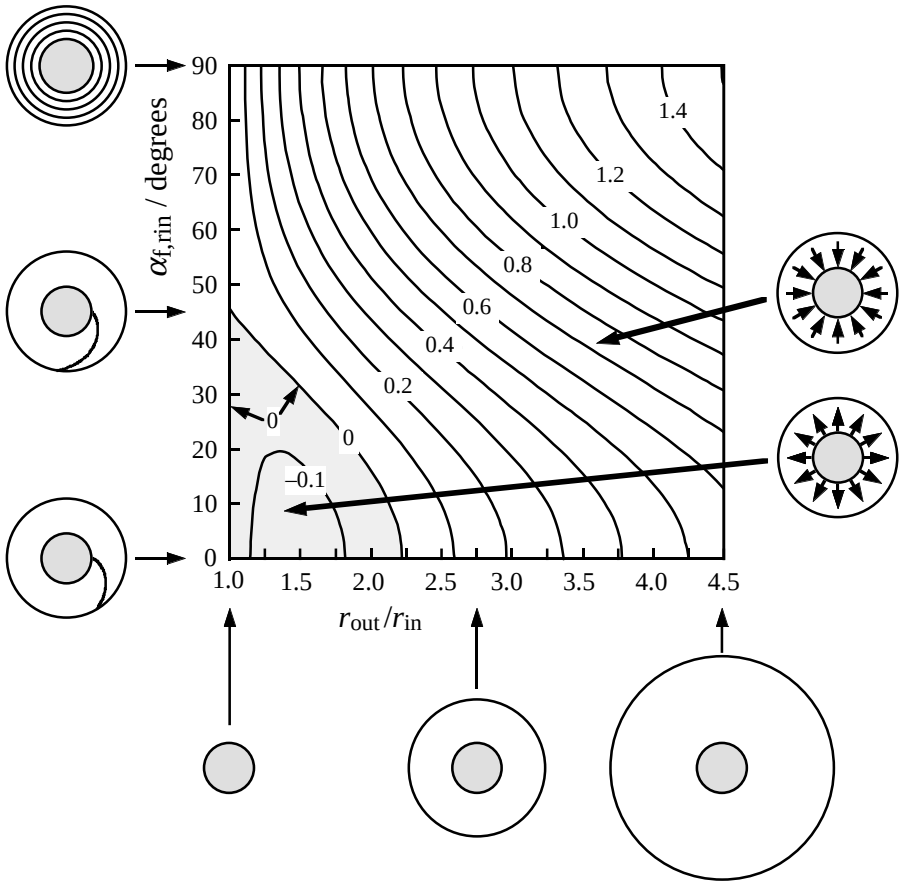

Figure 7. Contours of equal normal stress divided by the muscle stress σ_f (assumed uniform over the muscle volume) exerted by the accelerator muscle on the entoglossal process. Each point in the plot shows a unique design combination of $\alpha_{f,r_{in}}$ and r_{out}/r_{in}. Pictograms depict cross-sections of entoglossal process (grey) and muscle (white). Horizontal axis: ratio of outer and inner radius. From left to right, the relative muscle thickness increases, as indicated by the bottom row of pictograms. Vertical axis: internal muscle fibre angle increases from (bottom) 0 to (top) 90°. Fibre trajectories change according to optimum packing requirement as indicated by left row of pictograms. The normal stress is positive in the white area of the plot (as illustrated by inward pointing arrows in top right pictogram). The normal stress is negative in the grey area of the plot (illustrated by outward pointing arrows in associated pictogram).

stress on the entoglossal process. This is expected to allow muscle elongation without too high a frictional counter force. An exact quantitative treatment of this aspect is not yet possible (caused by insufficient kowledge about the lubricant).

Finally, consider the distribution of muscle fibre strain with prescribed and simplified deformations. Consider a short ring of accelerator muscle tissue with initial inner radius $r_{in,0}$, initial outer radius r_0, and initial length h_0 (figure 8). Let these initial values now change (through a combination of radial contraction and elongation) to r_{in}, r, and h, respectively. The ring is not allowed to make a shearing deformation in the longitudinal direction. The tissue is assumed to be incompressible, so that the volume of the muscular ring must be conserved. Hence,

$$\pi(r_0^2 - r_{in,0}^2)h_0 = \pi(r^2 - r_{in}^2)h. \tag{20}$$

By rewriting (20), the new local radius is obtained:

$$r = \sqrt{r_{in}^2 + (r_0^2 - r_{in,0}^2)(h_0/h)}. \tag{21}$$

The strain in the radial direction can now be computed (by assuming local conservation of volume) as

$$\varepsilon_r = \frac{\mathrm{d}(r - r_0)}{\mathrm{d}r_0} = \frac{1}{\sqrt{r_{in}^2 + (r_0^2 - r_{in,0}^2)(h_0/h)}} \frac{h_0 r_0}{h} - 1. \tag{22}$$

Similarly, the strain in the tangential (circumferential) direction is given by

$$\varepsilon_t = \frac{r - r_0}{r_0}. \tag{23}$$

From these two strain values, the strain in the muscle fibre direction can be computed. Consider an infinitesimally short fibre segment with length $\mathrm{d}r_0$ in the radial direction (figure 8). The associated tangential segment length $\mathrm{d}t_0$ is $\mathrm{d}r_0 \tan\alpha_{f,0}$ and the fibre segment length $\mathrm{d}s_{f,0}$ is $\mathrm{d}r_0/\cos\alpha_{f,0}$. After the deformation, $\mathrm{d}r_0$ has changed to $\mathrm{d}r = \mathrm{d}r_0 + \varepsilon_r\,\mathrm{d}r_0$, while $\mathrm{d}t_0$ has changed to $\mathrm{d}t = \mathrm{d}t_0 + \varepsilon_t\,\mathrm{d}t_0$. Then, the local muscle fibre strain can be obtained from

$$\varepsilon_f = \frac{\sqrt{(\mathrm{d}r)^2 + (\mathrm{d}t)^2} - \mathrm{d}s_{f,0}}{\mathrm{d}s_{f,0}}. \tag{24}$$

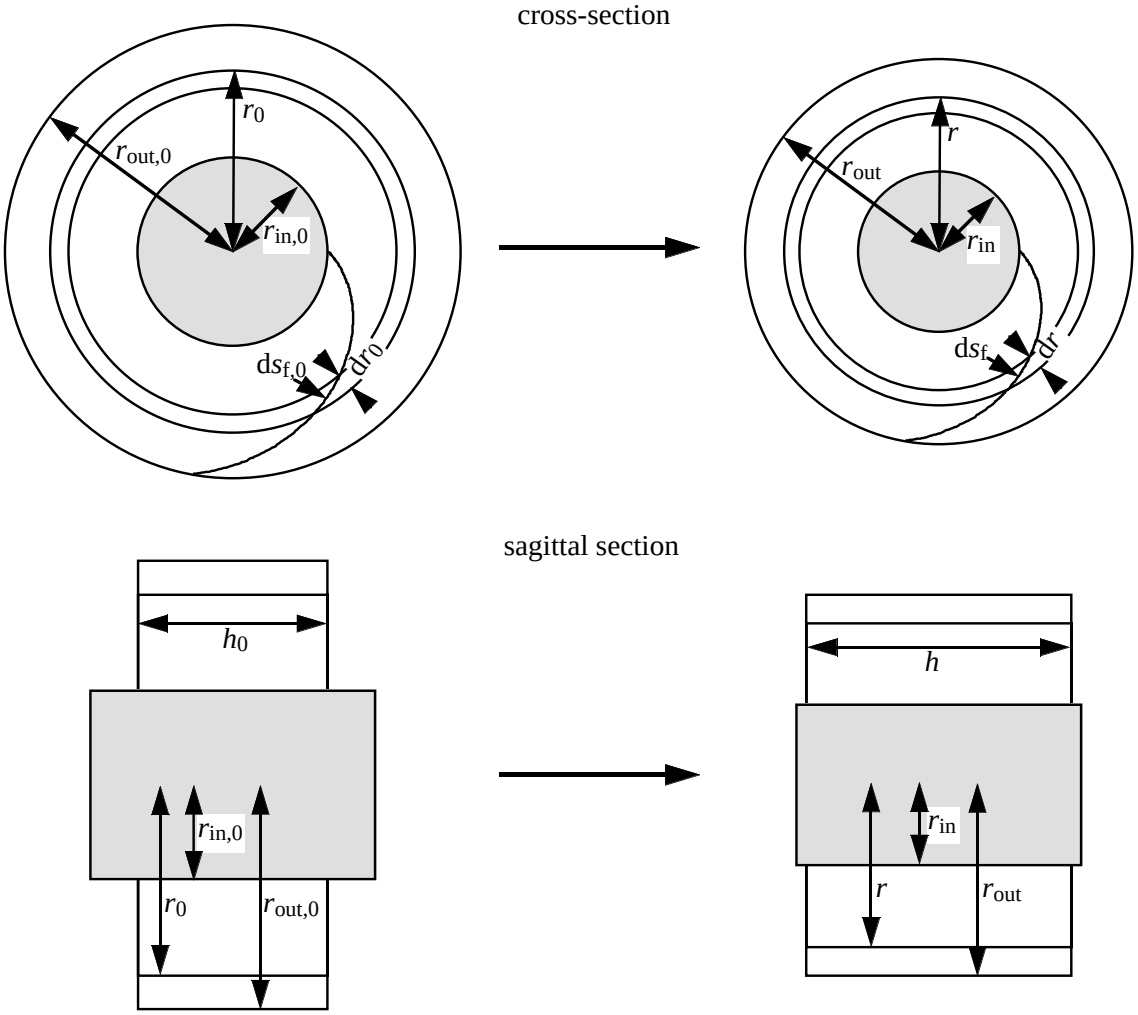

Figure 8. Illustration of simple deformations used to calculate muscle fibre strains. Top, cross-sections; bottom, sagittal sections. Left side, initial shape; right side, deformed shape. Grey area, entoglossal process; white area, accelerator muscle. Symbols are explained in Appendix 1. Further explanations in main text.

Unfortunately, *in vivo* strain measurements are not available for the accelerator muscle. Measurements by Wainwright & Bennett (1992*b*) with an *in vitro* preparation make it, however, likely that a considerable longitudinal strain may be generated.

Figure 9*a* shows how the muscle fibre strain varies with r if the local longitudinal muscle strain is 0.4 (i.e. $h/h_0 = 1.4$), while r_{in} is kept constant and any shearing in the longitudinal direction is avoided. For this simple deformation $\varepsilon_f \leq 0$. Clearly, the strain variation with r depends strongly on the initial value of $\alpha_{f,r_{in}}$. The least variation with r is found with an initial value for $\alpha_{f,r_{in}}$ of about 45°. For $\alpha_{f,r_{in}} = 90°$, the strain approaches zero if r approaches r_{in}. For $\alpha_{f,r_{in}} = 0°$, the strain becomes strongly negative towards r_{in}. The elongation of the muscle segment corresponds to increasing values of α_f, except for $\alpha_{f,r_{in}} = 90°$ and for $\alpha_{f,r_{in}} = 0°$ at the inner muscle boundary where the angles are constant. In conclusion, a fairly uniform strain (and presumably work output) can only be achieved if $\alpha_{f,r_{in}}$ is approximately 45°. During muscle lengthening, however, r_{in} will probably decrease owing to a thinning of the internal collagenous sheet (if this sheet lengthens also) and finally the sliding over the tapered portion of the entoglossal bone. It is therefore useful to examine the effect of a decrease of r_{in} on the strain distribution.

Figure 9*b* shows how the muscle fibre strain varies with r if r_{in} is chosen to be $0.85r_{in,0}$, whereas the longitudinal strain is zero ($h = h_0$). Now, at the inner muscle boundary *positive* strains are present for $\alpha_{f,r_{in}} > 50°$. Thus, the central parts of the muscle would absorb energy with the prescribed deformation if they were to exert any muscle fibre tension. An angle of approximately 50° gives the least variation in muscle fibre strain with a variation of r. Large values of $\alpha_{f,r_{in}}$ lead to relatively large contractions in the central muscle parts. The decrease in r_{in} corresponds to decreasing values of α_f, except again for $\alpha_{f,r_{in}} = 90°$ and for $\alpha_{f,r_{in}} = 0°$ at the inner muscle boundary where the angles are constant.

Now, it is interesting to examine a combination of muscle elongation ($h/h_0 = 1.4$) and a decrease in the inner muscle radius $r_{in} = 0.85r_{in,0}$. Figures 9*c*, *d* show that muscle fibre strain is now remarkably constant, even with inner fibre angles of 0 and 90° (an

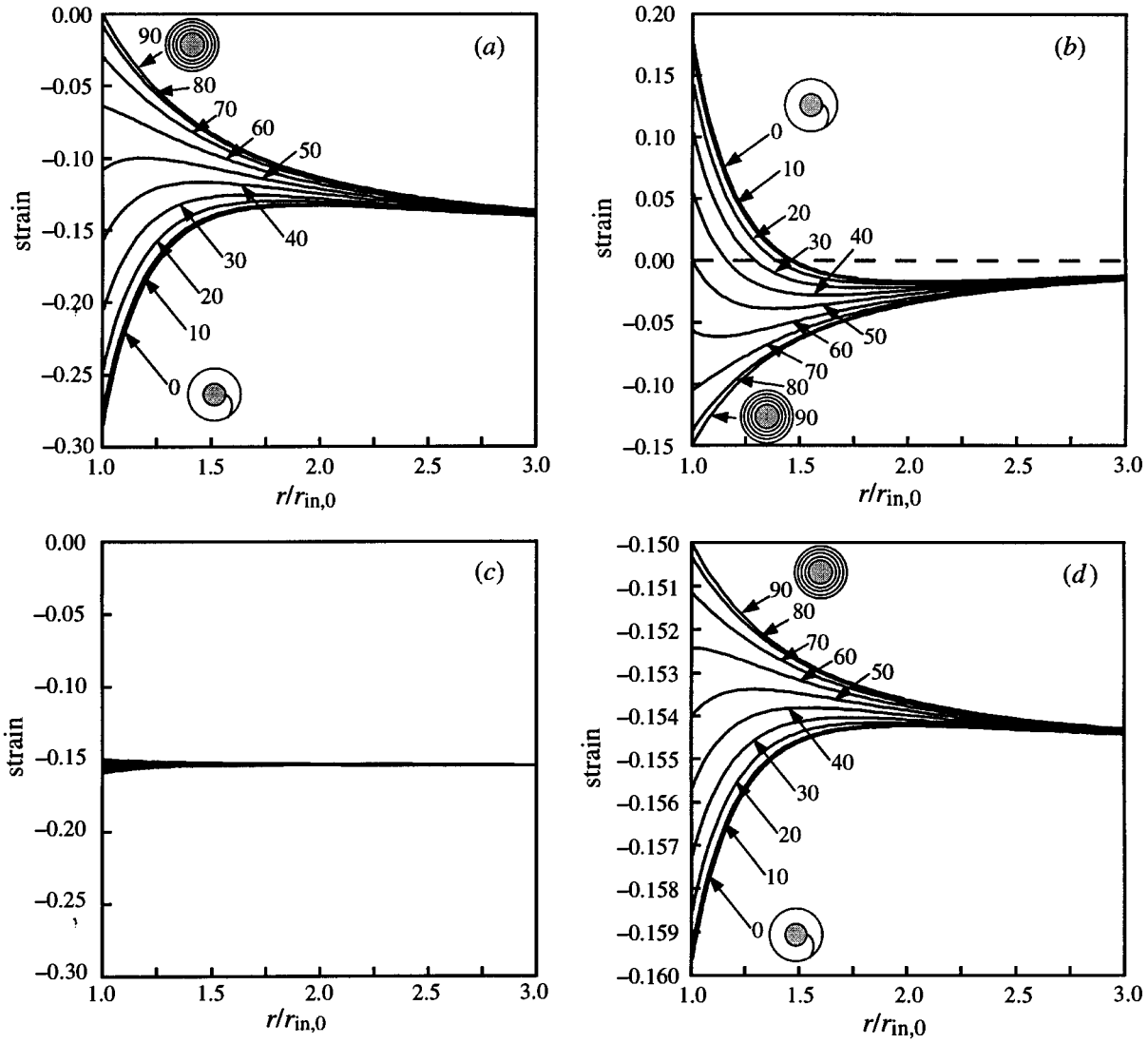

Figure 9. In each panel, a family of strain curves is shown with the initial inner muscle-fibre angle $\alpha_{\mathrm{f},r_{\mathrm{in}}}$ indicated in degrees. Pictograms for $\alpha_{\mathrm{f},r_{\mathrm{in}}} = 0$ and 90° depict cross-sections of entoglossal process (grey) and muscle (white) with muscle fibre path(s). The horizontal axes show the non-dimensional ratio $r/r_{\mathrm{in},0}$, where r is the distance of a point in the accelerator muscle to the muscle centre. (*a*) Muscle fibre strain as a consequence of a strain of 0.4 in the longitudinal direction. (*b*) Muscle fibre strain as a consequence of a 15% reduction in r_{in}. (*c*) Muscle fibre strain as a consequence of a strain of 0.4 in the longitudinal direction and a 15% reduction in r_{in}, same scale as in (*a*). (*d*) The same curves as in (*c*), but at a higher resolution.

angle of about 45° would again yield the best result). The strain distribution can be made almost perfectly uniform if r_{in} is made slightly smaller than $0.85r_{\mathrm{in},0}$. Thus, the muscle fibre strain can be made uniform for every $\alpha_{\mathrm{f},r_{\mathrm{in}}}$ if the right combination is chosen of elongation and change in inner muscle radius. Figure 9*c*, *d* shows just one example out of a continuous range of combinations of longitudinal strain and change in inner radius that yields this result. This is further exemplified by the contour plots of figure 10 for a muscle with $r_{\mathrm{out}}/r_{\mathrm{in}} = 2.5$ and an initial $\alpha_{\mathrm{f},r_{\mathrm{in}}}$ of 30°. Figure 10*a* shows contours with a constant standard deviation in the muscle fibre strain over the cross-section. The fat contour with arrow heads shows the deformational path with, at each instant, a uniform strain over the cross-section. Of course, the muscle fibre strain decreases along the contour in the direction of the arrows. Interestingly, this deformational path corresponds exactly to a constant normalized normal stress ($\sigma_{\mathrm{n}}^{*} = \sigma_{\mathrm{n}}/\sigma_{\mathrm{f}}$; cf. figure 10*b*) and constant fibre angles with the radial direction in each material point (figure 10*c*, *d*). Deviations to the right of this special deformational route result in an increase in σ_{n}^{*} and in decreasing values of α_{f}. A reverse effect is present for deviations to the left.

Experiments are required to see which options the chameleon actually uses during prey capture. Muscle portions that extend beyond the tip of the entoglossal process do still have a significant internal radius due to the presence of the internal collagenous sheet. The dimensions of the sheet are probably important to establish a favourable combination of muscle elongation and radial contraction.

PHILOSOPHICAL TRANSACTIONS OF THE ROYAL SOCIETY B BIOLOGICAL SCIENCES

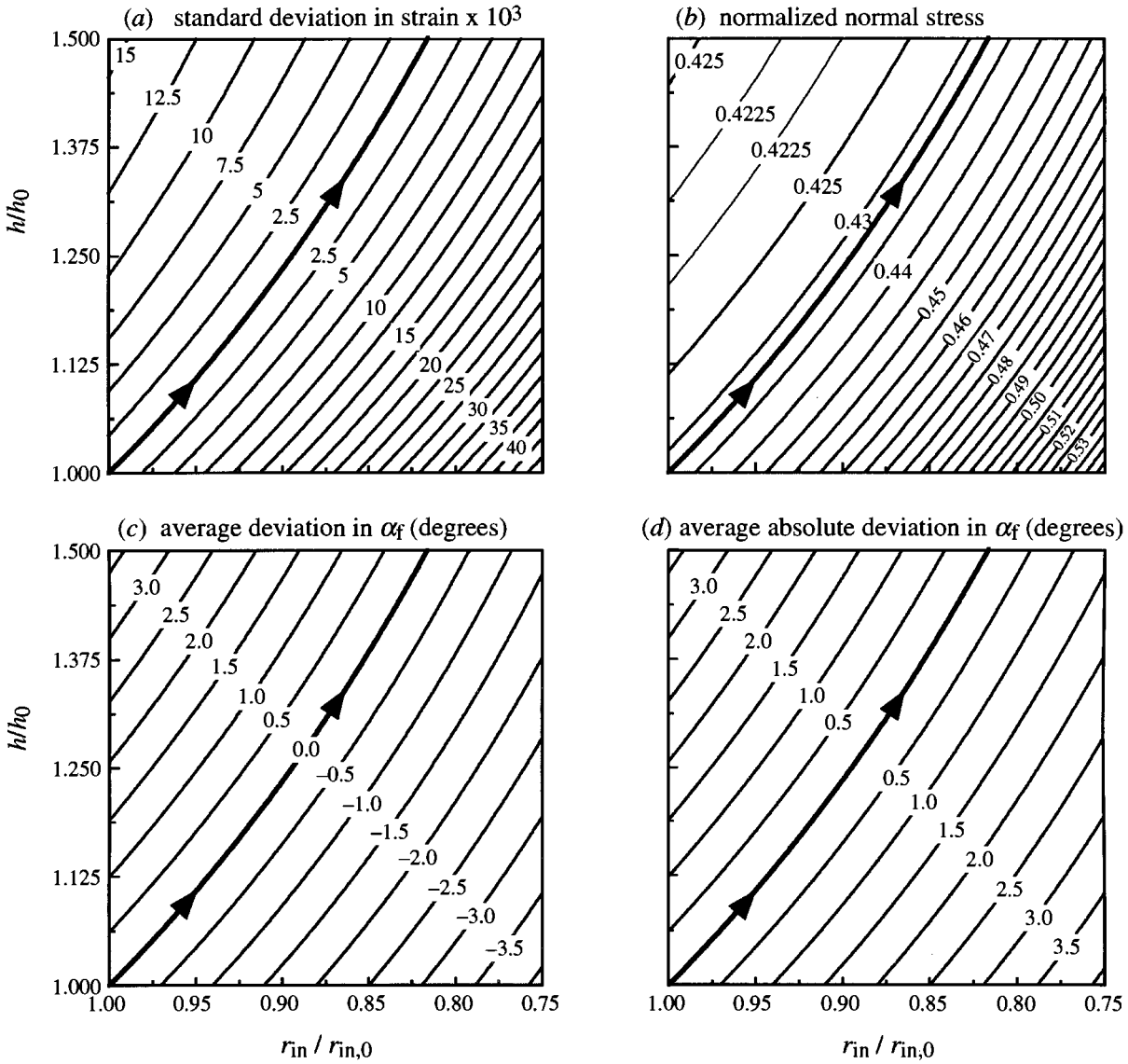

Figure 10. Contour plots showing how various parameters are influenced by an arbitrary change in the inner radius ($r_{in}/r_{in,0}$, horizontal axis) and the length of a muscle segment (h/h_0, vertical axis). For each panel, $r_{out,0}/r_{in,0} = 2.5$ and the initial $\alpha_{f,r_{in}} = 30°$. The deformational constraints of figure 8 are used and the muscle fibre stress σ_f is the same over the cross-section. (*a*) Contours show values of standard deviation in the strain times 10^3 over the muscular cross-section. The fat contour with the arrow heads shows the deformational path that results in the same strain over the cross-section (it should, however, be realized that the strain varies along this path). (*b*) Contours show values of the normalized normal stress on the entoglossal process (σ_n/σ_f). The contour with the arrow heads in panel (*a*) is plotted also in (*b*), showing that this path corresponds to a path with a constant normalized normal stress. Note the valley in the contour plot close to the upper left-hand side corner. (*c*) Contours show the deviation in the fibre angle α_f from the initial value $\alpha_{f,0}$, averaged over the cross-section. The path of the replotted fat contour from (*a*) corresponds now to the zero contour. (*d*) Similar contour plot as (*c*), but now for the absolute deviation, showing that the zero contour of panel (*c*) corresponds indeed with a deformational path with a constant fibre angle in each material point.

3. DISCUSSION

The model analysis predicts that the muscle fibres' shapes and orientations in the accelerator muscle of the Chameleon tongue allow (1) a close packing of myofibrils and (2) a fairly homogeneous strain along the fibres. Compared to a muscle fibre arrangement of a typical sphincter with concentric layers of circular muscle fibres, the chameleon fibre architecture results in a relatively high intramuscular pressure and a relative low normal stress at the internal boundary.

It seems favourable if the muscle fibres operate with an approximately uniform strain along their length. As shown in the previous section, this is most easily realized with an internal fibre angle $\alpha_{f,r_{in}}$ of about 45°. With the right combination of muscle elongation and change in internal radius, a uniform strain can also be obtained with other values of $\alpha_{f,r_{in}}$. During the initial phase of tongue acceleration, however, the muscle presumably elongates with only a very small change in r_{in} (due to thinning of the inner tendinous sheet). Therefore, acceptable values for $\alpha_{f,r_{in}}$ should not deviate too much from 45°, and indeed the histological section shown by Gans (1967)

shows that, for most fibres (figure 5*h*) $\alpha_{f,r_{in}} \approx 45°$.

It is advantageous if the intramuscular pressure is on average very high, because this helps to generate a strong pressure gradient in the forward direction and hence a high forward acceleration. This is best achieved with small values of $\alpha_{f,r_{in}}$ (cf. figure 6*b*). This effect may shift the optimal value of 45° for an equal strain to somewhat lower values. Values in the range of 30–45° can be observed in several histological sections from the literature (e.g. Gans 1967; Bell 1989).

The optimal relative thickness of the outer and inner radius (r_{out}/r_{in}) along the accelerator muscle cannot at present be predicted. This can only be done if a forward dynamics model is developed. In a forward dynamics model, movements are calculated from a prescribed mechanical stress distribution, or, even better, a prescribed activation distribution of the muscular system. An example of such a model for a similar system is the squid tentacle model of Van Leeuwen & Kier (1997). At present, I will limit myself to a short qualitative discussion of optimal muscle thickness.

First, to allow an effective longitudinal sliding of the accelerator muscle over the entoglossal process the normal stress on the process should not be too high. On the other hand, the normal stress should be high enough to enable an effective acceleration over the tapering end of the process. These demands are expected to limit the range of acceptable values of r_{out}/r_{in}.

Second, the muscle should be thick enough to push the associated effective tongue mass forward. It should, however, not be oversized since then other muscle portions would have to push (or to pull) forward too large of a mass. This would reduce the acceleration and peak velocity of the tongue pad.

In conclusion, the boundaries for an acceptable design region of r_{out}/r_{in} cannot yet be predicted exactly because of (i) the limited good quantitative morphological and physiological data about the accelerator muscle, the associated internal collagenous sheet and lubricant, and the exact shape of the entoglossal process, and (ii) the lack of a validated forward dynamics model of tongue projection. A forward dynamics model could also show how the tongue projection musculature should be optimally controlled. In addition, it could be used to see whether it is advantageous if the accelerator muscle is tapered from the base to the tip. The load on the basal portion seems to be greatest because here the largest mass must be pushed forward, especially during the initial elongation phase of the strike. This can be compensated for by a relatively large cross-sectional area or by relatively long myosin filament lengths (cf. Van Leeuwen 1991; Van Leeuwen & Kier 1997). The relative invariance of the myosin filament length in vertebrates suggests the first option. Histological sections indeed show greater cross-sectional areas for more basal positions. In contrast, in the tentacles of the squid, the second possibility is predicted (cf. Van Leeuwen & Kier 1997).

In the close packing analysis of the modelling section, I neglected the space occupied by nerves, blood vessels, connective tissue, etc. With a non-homogeneous distribution of these tissue components, slightly different shapes of the muscle fibre trajectories would be predicted. Quantitative histological observations are required to investigate these aspects.

In a tongue preparation of *Chamaeleo jacksonii* Boulenger, Wainwright & Bennett (1992*b*) replaced the entoglossal process by a stiff glass tube filled with saline solution, with an open lumen. The accelerator muscle was stimulated electrically and the pressure inside the glass tube was measured. This recorded pressure is equivalent to the normal stress on the entoglossal process as defined in the present paper. The recorded peak pressure of about 11 kPa is remarkably low compared with the calculated peak *intramuscular* pressures in the tentacle of a squid (about 20 kPa, cf. Van Leeuwen & Kier 1997). In the squid, this high intramuscular pressure is produced with relatively short sarcomeres that generate only relatively low tensile stresses. As explained in the modelling and results section, the *luminal* pressure in the chameleon is expected to be much lower than the highest intramuscular pressure. This is due to the outwardly directed tensile stress component of the muscle fibres at the inner boundary (third term in equation (19)). Thus, I expect also that the intramuscular pressure adjacent to the inner boundary of the accelerator muscle can be considerably greater than the exerted normal stress on the entoglossal bone (or the pressure exerted in the lubricant layer). It seems also probable, given the difference in myofilament length, that a higher peak intramuscular pressure is generated in the tongue of the chameleon than in the tentacle of the squid. A decreasing internal radius of the accelerator muscle is expected (according to equation (19) and figure 7) to lead to an increasing normal stress on the underlying structures. This effect is likely to be used in the final acceleration phase over the tapering tip of the entoglossal process.

From the present analysis, it is clear that the accelerator muscle is not a typical sphincter muscle. Compared to a sphincter of similar dimensions and muscle fibre tensile stress, it generates a higher intramuscular pressure and a lower normal stress at the internal boundary. The muscle fibre arrangement allows also fairly uniform strains to be generated along the muscle fibres, and it excludes significant torsional motions.

In the model analysis, I have ignored shearing deformations in the longitudinal direction. The pressure calculations show that the highest pressures are produced adjacent to the entoglossal process. Therefore, adjacent to the process the strongest longitudinal pressure gradient is expected and thus the strongest forward acceleration. I expect therefore that the outer layers will lag somewhat behind the inner muscle layers (if the sliding friction is indeed kept low). The reaction force from the tapering tip of the process will also tend to accelerate most directly the innermost muscle layers. A detailed experimental

PHILOSOPHICAL TRANSACTIONS OF THE ROYAL SOCIETY B BIOLOGICAL SCIENCES

analysis in combination with a theoretical dynamic multicompartment analysis are required to examine these issues. At present, the importance of taper of the entoglossal process for tongue extension cannot be established quantitatively.

The accelerator muscle of the chameleon tongue is an example of a design with muscle fibres with a varying curvature along their length and predicted pressure contours at an angle to the local muscle fibre direction. The angle between fibres and contours can be as much as 60° at the inner boundary of the muscle. This is different from the architectural models of unipennate and bipennate skeletal muscles by Van Leeuwen & Spoor (1992, 1993). Their goal was to demonstrate the importance of the application of the principle of mechanical stability for the understanding of muscle shape. For this purpose, the simplest models were designed with a constant curvature for each muscle fibre and pressure contours aligned with the muscle fibres. Thus, mechanical stability can generally be applied, but pressure contours are in general not parallel to the muscle fibre direction, although for many muscles a parallel orientation will be a very good approximation of the real situation.

The second extreme design option with radially arranged muscle fibres was judged to be inappropriate for the accelerator muscle because it would result in a negative normal stress on the entoglossal process (equation (6)). However, several muscular hydrostats with a central liquid filled lumen have radially arranged muscle fibres. Such an arrangement is very appropriate for the production of a negative luminal pressure, and is, for example, used by octopods to adhere to prey with their suckers (Kier & Smith 1990) and by nematodes to suck in food with their muscular pharynx (Albertson & Thomson 1976).

4. CONCLUSIONS

The following conclusions can be drawn from the present analysis.

(1) The architectural model proposed here for the accelerator muscle of the chameleon tongue makes it likely that the typically curved muscle fibre trajectories are shaped according to a close packing principle.

(2) Significant torsional motions can be prevented since half of the muscle fibres run clockwise and the other half anticlockwise.

(3) The muscle fibre arrangement allows fairly uniform strains to be generated along the length of the muscle fibres.

(4) The special muscle fibre arrangement in the accelerator muscle results in relatively high intramuscular pressures and relatively low normal stresses at the internal boundary.

(5) The present model predicts the decreasing diameter of the entoglossal process to have a positive effect on the normal stress development of the muscle on the process. This is expected to support a rapid final acceleration over the entoglossal tip.

Professor R. McN. Alexander (Leeds), Professor R. Blickhan (Jena), Mr M. Heldoorn (Leiden), Dr T. Johansson (Jena), Dr W. M. Kier (Chapel Hill), Dr M. Muller (Wageningen) and Dr C. W. Spoor (Rotterdam) are thanked for useful comments on a draft of this paper. I had stimulating discussions with my colleagues in Jena. Professor R. Blickhan is thanked for his invitation to work in Jena. Dr P. C. Wainwright kindly agreed that figure 2 from Wainwright & Bennett (1992*a*) could be adapted for portions of figure 1. This work was supported by grant DFG INK 22/A1-1, TP A3 from the Deutsche Forschungsgemeinschaft.

APPENDIX 1. SYMBOLS AND DEFINITIONS

Symbols denoted with an asterisk (∗) represent normalized quantities.

symbol	definition
a_r	acceleration in radial direction.
c_f	local curvature of muscle fibre, $c_\mathrm{f} = 1/R_\mathrm{f}$.
c_f^*	non-dimensional curvature of muscle fibre, $c_\mathrm{f}^* = c_\mathrm{f} r_\mathrm{in}$.
d_f	width of muscle fibre in transverse plane.
$\mathrm{d}r$	radial length of infinitesimal muscle segment.
$\mathrm{d}r_0$	initial radial length of infinitesimal muscle segment.
$\mathrm{d}s_{\mathrm{f},0}$	initial length of infinitesimal muscle fibre segment.
$\mathrm{d}t$	circumferential length of infinitesimal muscle segment.
$\mathrm{d}t_0$	initial circumferential length of infinitesimal muscle segment.
$g_\mathrm{f} = g_\mathrm{f}(r)$	arc length of circle sector of radius r by which a muscle fibre is traversed.
$g_{\mathrm{f},r_\mathrm{in}}$	attachment length of a muscle fibre in transverse plane at inner muscle boundary.
h	width of muscle segment in longitudinal muscle direction.
h_0	initial width of muscle segment in longitudinal muscle direction.
h_f	width of muscle fibre in longitudinal muscle direction.
$p = p(r)$	intramuscular pressure in accelerator muscle.
p^*	normalized intramuscular pressure, $p^* = p/\sigma_\mathrm{f}$.
p_{r_in}	intramuscular pressure in accelerator muscle at inner boundary.
p_{r_out}	intramuscular pressure in accelerator muscle at outer boundary.
p_1	local intramuscular pressure in sphincter muscle.
p_{1,r_in}	intramuscular pressure in sphincter muscle at inner boundary.
p_{1,r_out}	intramuscular pressure in sphincter muscle at outer boundary, $p_{1,rout} = 0$.
p_2	intramuscular pressure in accelerator muscle with straight and radially directed muscle fibres.
r	radial coordinate, $r = 0$ at centre of muscle and centre of entoglossal process.
r_0	initial outer radius of thin muscle ring in accelerator muscle.
R_f	local radius of curvature of muscle fibre.
r_in	inner radius of accelerator muscle.
$r_{\mathrm{in},0}$	initial inner radius of accelerator muscle.

r_{out}	outer radius of accelerator muscle.
$r_{\mathrm{out},0}$	initial outer radius of accelerator muscle (figure 8).
s_{f}	curvilinear coordinate along muscle fibre.
$\alpha_{\mathrm{f}} = \alpha_{\mathrm{f}}(r)$	local angle of muscle fibre with radial direction.
$\alpha_{\mathrm{f},0}$	α_{f} before muscular deformation.
$\alpha_{\mathrm{f},r_{\mathrm{in}}}$	angle of muscle fibre with radial direction at $r = r_{\mathrm{in}}$.
$\alpha_{\mathrm{f},r_{\mathrm{out}}}$	angle of muscle fibre with radial direction at $r = r_{\mathrm{out}}$.
β	angle of surface of entoglossal process with central axis.
ε_{f}	strain in muscle fibre direction.
ε_r	strain in radial direction.
ε_t	strain in circumferential direction.
γ	sector angle of infinitesimal muscle segment (figure 3).
ρ	density of muscle tissue.
σ_{f}	tensile muscle fibre stress.
σ_{l}	longitudinal muscle fibre stress.
σ_{n}	normal stress on entoglossal process.
$\sigma_{\mathrm{n}}^* = \sigma_{\mathrm{n}}/\sigma_{\mathrm{f}}$	normalized normal stress on entoglossal process.
$\sigma_{\mathrm{n},1}$	normal stress on entoglossal process by sphincter muscle.
$\sigma_{\mathrm{n},2}$	normal stress on entoglossal process by muscle with fibres oriented in radial direction.
σ_{s}	shear stress with entoglossal process.
σ_{tot}	stress from entoglossal process on accelerator muscle.
θ_{f}	for a particular muscle fibre, the angle between the radial direction at r and the radial direction at r_{in} ($\theta_{\mathrm{f}} \geq 0$).

APPENDIX 2. PRESSURE GRADIENT FORMULAE

Here, expressions are derived for the pressure gradient of accelerator muscle design 2 (all muscle fibres in radial direction) and the close packing design with complex fibre curvatures.

Figure 3*a* shows a cross-section of the design 2 accelerator muscle, with internal and external radii. An infinitesimally small muscle segment is drawn which is specified by the infinitesimally small sector angle γ, outer radius r, inner radius $r - \mathrm{d}r$, and length h. The mass of the segment is equal to $\rho\gamma hr\,\mathrm{d}r$, where ρ is the density of the tissue. Figure 3*b* shows the segment in expanded form with the forces parallel to the mid-radial direction acting on it. The force components can be divided in pressure forces and fibre stress forces. At the two lateral sides, only pressure forces act because the fibres run in radial directions only. The sum of the force components should be equal to the radial acceleration a_{r} of the segment times its mass. Hence,

$$\begin{aligned}&\gamma rh\left(-p+\sigma_{\mathrm{f}}\frac{r_{\mathrm{in}}}{r}\right)\\&+\gamma(r-\mathrm{d}r)h\left(p-\mathrm{d}p-\sigma_{\mathrm{f}}\frac{r_{\mathrm{in}}}{r-\mathrm{d}r}\right)\\&+h\,\mathrm{d}r(2p-\mathrm{d}p)\sin(\gamma/2)=a_r\rho\gamma hr\,\mathrm{d}r,\end{aligned}\quad(25)$$

where the third term is obtained by adding the two lateral force components of figure 3*b*. Formula (25) can be simplified by assuming $\sin(\frac{1}{2}\gamma) = \frac{1}{2}\gamma$ and subsequently eliminating h and γ:

$$\begin{aligned}&r\left(-p+\sigma_{\mathrm{f}}\frac{r_{\mathrm{in}}}{r}\right)+(r-\mathrm{d}r)\left(p-\mathrm{d}p-\sigma_{\mathrm{f}}\frac{r_{\mathrm{in}}}{r-\mathrm{d}r}\right)\\&+\mathrm{d}r\,(p-\tfrac{1}{2}\mathrm{d}p)=a_r\rho r\,\mathrm{d}r.\end{aligned}\quad(26)$$

Rearranging and adding various terms of (26), and ignoring the $\mathrm{d}p\,\mathrm{d}r$ term, it follows that

$$\mathrm{d}p = -a_r\rho\,\mathrm{d}r. \quad(27)$$

To estimate the importance of the acceleration term, consider the pressure at radius r in the muscle tissue:

$$p_{2,r} = \sigma_{\mathrm{f}}\frac{r_{\mathrm{in}}}{r_{\mathrm{out}}} - \int_{r_{\mathrm{out}}}^{r}\rho a_r\,\mathrm{d}r. \quad(28)$$

Taking $r_{\mathrm{in}} = 2.5$ mm, $r_{\mathrm{out}} = 6.25$ mm, $\sigma_{\mathrm{f}} = 100$ kPa, $\rho = 1050\ \mathrm{kg\,m^{-3}}$, and assuming a high inward acceleration of $-200\ \mathrm{m\,s^{-2}}$ throughout the muscle tissue, the first term of (28) is approximately 51 times greater at the inner boundary of the muscle than the absolute value of the second term. Therefore, for the present purposes it is allowed to assume the pressure to be uniform in a cross-section, $\mathrm{d}p = 0$. This is equivalent to the assumption that tissues in the interfibre spaces cannot withstand a pressure gradient in the radial direction (with zero acceleration).

A similar calculation can now be made for the accelerator muscle with a close packing design. Figure 3*c* shows again a cross-section of the accelerator muscle, with a curved muscle fibre path. A similar infinitesimally small muscle segment is defined as in figure 3*a*. Figure 3*d* shows the segment in expanded form with the forces parallel to the midradial direction acting on it. The force components can be divided in pressure forces and fibre stress forces. Now, at the two lateral sides, fibre stresses also act because the muscle fibre angle is greater than zero. It is assumed that no net fibre force acts parallel to the lateral surface because of equal numbers of fibres in clockwise and anticlockwise directions. The various force components should again be equal to the acceleration of the segment times its mass:

$$\begin{aligned}&\gamma rh(-p+\sigma_{\mathrm{f}}\cos^2\alpha_{\mathrm{f}})\\&+\gamma(r-\mathrm{d}r)h(p-\mathrm{d}p-\sigma_{\mathrm{f}}\cos^2\alpha_{\mathrm{f}})\\&+h\,\mathrm{d}r(2p-\mathrm{d}p-2\sigma_{\mathrm{f}}\sin^2\alpha_{\mathrm{f}})\sin(\gamma/2)\\&=a_r\rho\gamma hr\,\mathrm{d}r.\end{aligned}\quad(29)$$

A similar treatment as for equation (25) leads to (wherein it should be recognized that α_{f} depends on r):

$$\mathrm{d}p = -\frac{\sigma_{\mathrm{f}}}{r}\,\mathrm{d}r - a_r\rho\,\mathrm{d}r. \quad(30)$$

The greatest influence of the second term of the right-hand side in (30) can be expected at the peripheral boundary, whereas the first term makes its smallest contribution (with a constant muscle fibre stress). Taking for this position $r = 6.25$ mm and the same values for the other parameters as above, it follows that the absolute value of the first term is approximately 76 times greater than that of the second term. By neglecting the second term, equation (17) is obtained.

REFERENCES

Abbott, B. C. & Baskin, R. J. 1962 Volume changes in frog muscle during contraction. *J. Physiol.* **161**, 379–391.

Albertson, D. G. & Thomson, J. N. 1976 The pharynx of *Caenorhabditis elegans*. *Phil. Trans. R. Soc. Lond.* B **275**, 299–325.

Altevogt, R. & Altevogt, R. 1954 Studien zur Kinematik der Chamäleonenzunge. *Z. Vergl. Physiol.* **36**, 66–77.

Bell, D. A. 1989 Functional anatomy of the chameleon tongue. *Zool. Jb. Anat.* **119**, 313–336.

Bell, D. A. 1990 Kinematics of prey capture in the chameleon. *Zool. Jb. Physiol.* **94**, 247–260.

Brücke, E. 1852 Über die Zunge der Chamäleonen. *Sitz. Ber. Math.-Nat. Kl. Akad. Wiss., Wien* **8**, 62–70.

Duvernoy, G. L. 1836 Sur les mouvements de la langue du caméléon. *C.R. hebd. Sánc. Acad. Sci., Paris* **2**, 349–351.

Gans, C. 1967 The chameleon. *Nat. Hist.* **76**, 52–59.

Gnanamuthu, C. P. 1930 The anatomy and mechanism of the tongue of *Chamaeleo carcaratus* (Merrem). *Proc. Zool. Soc. Lond.* **31**, 467–486.

Gnanamuthu, C. P. 1937 Comparative study of the hyoid and tongue of some typical genera of reptiles. *Proc. Zool. Soc. Lond.* B **107**, 1–63.

Houston, J. 1828 On the structure and mechanism of the chameleon tongue. *Trans. R. Irish Acad.* **15**, 177–201.

Kier, W. M. & Smith, A. M. 1990 The morphology and mechanics of octopus suckers. *Biol. Bull. Mar. Biol. Lab.* **178**, 126–136.

Van Leeuwen, J. L. 1991 Optimum power output and structural design of sarcomeres. *J. Theor. Biol.* **149**, 229–256.

Van Leeuwen, J. L. & Kier, W. M. 1997 Functional design of tentacles in squid: linking sarcomere ultrastructure to gross morphological dynamics. *Phil. Trans. R. Soc. Lond.* B **352**, 551–571. (Preceding paper.)

Van Leeuwen, J. L. & Spoor, C. W. 1992 Modelling mechanically stable muscle architectures. *Phil. Trans. R. Soc. Lond.* B **336**, 275–292.

Van Leeuwen, J. L. & Spoor, C. W. 1993 Modelling the pressure and force equilibrium in unipennate muscles with in-line tendons. *Phil. Trans. R. Soc. Lond.* B **342**, 321–333.

Wainwright, P. C. & Bennett, A. F. 1992*a* The mechanism of tongue projection in chameleons. I. Electromyographic tests of functional hypotheses *J. Exp. Biol.* **168**, 1–21.

Wainwright, P. C. & Bennett, A. F. 1992*b* The mechanism of tongue projection in chameleons. II. Role of shape change in a muscular hydrostat *J. Exp. Biol.* **168**, 23–40.

Wainwright, P. C., Kraklau, D. M. & Bennett, A. F. 1991 Kinematics of tongue projection in *Chameleo oustaleti*. *J. Exp. Biol.* **159**, 109–133.

Zoond, A. 1933 The mechanism of projection of the chameleon's tongue. *J. Exp. Biol.* **10**, 174–185.

Received 30 October 1996; accepted 25 February 1997

PHILOSOPHICAL TRANSACTIONS OF THE ROYAL SOCIETY B BIOLOGICAL SCIENCES